Key Engineering Materials *Online: 2014-06-18*
ISSN: 1662-9795, Vol. 616, pp 120-128
doi:10.4028/www.scientific.net/KEM.616.120

Chemical reactivity and cathode properties of $LaCoO_3$ on lanthanum silicate oxyapatite electrolyte

Shunya Mihara[1,a], Kiyoshi Kobayashi[2,b], Takaya Akashi[3,c], and Yoshio Sakka[2,d]

[1] Graduate School of Engneering, Hosei University, 3-7-2, Kajino-cho, Koganei, Tokyo 184-8584, Japan

[2]Materials Processing Unit, National Institute for Materials Science, 1-2-1, Sengen, Tsukuba, Ibaraki 305-0047, Japan

[3]Faculty of Bioscience and Applied Chemistry, Hosei University, 3-7-2, Kajino-cho, Koganei, Tokyo 184-8584, Japan

[a]MIHARA.Shunya@nims.go.jp, [b]KOBAYASHI.Kiyoshi@nims.go.jp, [c]akashi@hosei.ac.jp, [d]SAKKA.Yoshio@nims.go.jp

Keywords: SOFC, cathode, $LaCoO_3$, lanthanum silicate oxyapatite, chemical reactivity

Abstract. Chemical reactivity and cathode properties of $LaCoO_3$ were investigated using new oxide ion conductor, lanthanum silicate oxyapatite. The $LaCoO_3$ is found to be good candidate for cathode of the lanthanum silicate oxyapatite solid-electrolyte since no chemical reaction occurred between the $LaCoO_3$ and lanthanum silicate oxyapatite heating at 1273 K for 60 h in air. Based on electrochemical measurements, lower overpotential between the $LaCoO_3$ and lanthanum silicate oxyapatite was confirmed compared to the overpotential at YSZ/$LaCoO_3$ interface. From analysis on the extended interfacial conductivity as function of oxygen activity at the triple phase boundary at fixed temperature, the overpotential evaluated by impedance spectra is the rate limiting process by oxygen diffusion on the $LaCoO_3$ surface. Comparing to the bulk conductivity of $LaCoO_3$, the electrode resistance evaluated by impedance spectra was confirmed to be different from the electrical transport properties of the $LaCoO_3$ bulk.

1. Introduction

Lanthanum cobaltite with provskite structure ($LaCoO_3$) is famous mixed conductor by electron holes and oxide ions and is the candidate for applications to cathode for solid oxide fuel cell (SOFC) and oxygen permeable membrane [1-7]. Although the $LaCoO_3$ shows high performance as SOFC cathode when yttria stabilized zirconia (YSZ) is used as solid electrolyte [1, 2], decrease in the cathode performance with continuous SOFC operation condition. Cause of the decrease in the cathode performance is the formation of insulator phase, $La_2Zr_2O_7$, by the chemical reaction between the YSZ and $LaCoO_3$ [8-10]. Hence, it is necessary to replace the solid electrolyte from YSZ if one wants to utilize the excellent cathode property of $LaCoO_3$ for SOFC.

Lanthanoid silicate oxyapatites have known as new oxide ion conductors since Nakayama *et al.* have reported their high oxide ion conductivity from 1995 to 1998 [11-13]. In particular, the lanthanum silicate oxyapatite shows high oxide ion conductivity even in the ceramic electrolyte. In addition, the oxide ion conductivity of the lanthanum silicate oxyapatite is higher than the conductivity of YSZ below about 873 K because of its low activation energy [13, 14]. Hence, the lanthanum silicate oxyapatite is the candidate of the solid electrolyte material for middle temperature operation SOFC [15]. On the other hand, no research has been done to develop specified electrode materials for the lanthanum silicate oxyapatite. We focused on the $LaCoO_3$ which could not apply as cathode material on the YSZ electrolyte even though the $LaCoO_3$ itself has excellent potential.

In this study, the chemical reactivity at the $LaCoO_3$/lanthanum silicate oxyapatite interface and fundamental research on the cathode performance was investigated. For investigation of the cathode properties, we applied new analysis theory by extended interfacial conductivity [16, 17]. Based on this

approach, we discussed about an origin of the overpotential between the $LaCoO_3$/lanthanum silicate oxyapatite interface.

2. Experimental

2.1. Sample Preparation

The $LaCoO_3$ and lanthanum silicate oxyapatite were synthesized by the water-based sol-gel method [18-20]. The raw materials were lanthanum nitrate hexahydrate ($La(NO_3)_3 \cdot 6H_2O$, 99.9% purity, Nacalai Tesque, Inc., Japan), cobalt(II) nitrate hexahydrate ($Co(NO_3)_2 \cdot 6H_2O$, 99.9% purity, Kojundo Chem. Lab. Co. Ltd., Japan), amorphous silicon dioxide (99.8% purity, Wako Pure Chem. Industry Ltd., Japan), and citric acid (98% purity, Wako Chem. Industry Ltd., Japan).

The lanthanum nitrate hexahydrate and cobalt nitrate hexahydrate were separately dissolved in distilled water and the solutions were stocked in glass bottle. The concentrations of two aqueous solutions were titrated by chelatometric titration method [18-21]. The concentrations of both solutions were about 1 mol/l.

Procedures of the $LaCoO_3$ synthesis was following: Corresponding amount of the lanthanum nitrate and cobalt nitrate aqueous solutions were pipetted into a glass beaker and mixed by magnetic hot stirrer. Then, citric acid with the same mole amount to sum of the lanthanum and cobalt in mixed aqueous solution was dissolved in the mixed aqueous solution. The homogeneous dissolved solution was heated with stirring using magnetic hot stirrer. The aqueous solution was changed into a viscous gel by evaporation of excess water. The viscous gel was dried by further heating on the hot stirrer and then, the dried gel in the beaker was replaced to heating mantle. Ash-like residue was obtained by pylorisis of the dried gel about 673 K. Precursor powder was obtained from the ash-like residue by crashing into powder using agate mortar and pestle. The $LaCoO_3$ powder was prepared by heating of the precursor powder at 973 K for 3 h in air. The $LaCoO_3$ is denoted as LCO, hereinafter.

The procedures of the synthesis on lanthanum silicate oxyapatite were the same with the previous paper [18-20, 22]. The composition is $La_{9.50}(SiO_4)_6O_{2.25}$ which is denoted as LSO, hereinafter. The LSO precursor was pre-heated at 1273 K for 3 h in air to remove residual carbons. Then, the pre-heated powder was pressed into pellets with 20 mm diameter and about 1.5 mm thickness. Well sintered pellets were obtained by sintering at 1773 K for 6 h in air. After the sintering, the diameter of the pellets was about 16 mm.

2.2. Chemical reactivity

Separately synthesized LCO and LSO powders were mixed in weight ratio of one to one using agate mortar and pestle. Then, the mixed powder was placed in YSZ crucible and heated at 1273 K for 60 h in air. After the heat-treatment, the formed phase was confirmed by powder X-ray diffraction (XRD) analysis using RINT-2500 (Rigaku Co. Ltd., Japan). For comparison of the reactivity of LCO and electrolyte material, formed phase was also confirmed by mixture of LCO and YSZ after the same procedures.

2.3. Preparation of the LCO ink

For fabrication of LCO porous-electrode on the LSO electrolyte, it was necessary to control its particle size and homogeneous dispersion in organic medium. Hence, the LCO powder was homogenized by planetary ball mill using zirconia ball having diameter of 0.8 mm. Ethanol was used as medium. The rotation velocity and milling period were 1000 rpm and 2 h, respectively. After the milling, 1 wt% of polyethyleneimine versus to the weight of LCO powder was added into the LCO dispersed ethanol to avoid the aggregation of the LCO particles. Amount of LCO powder in this ink is about 0.05g / ml.

2.4. Preparations of the cell

Cathode properties of the LCO on LSO electrolyte were investigated by a half cell configuration. In order to fabricate the LCO electrode, both surfaces of the sintered LSO ceramics were polished using #100 to #2000 waterproof abrasive papers. In addition, thin groove was made using a diamond wheel for binding platinum wire.

Two polyester-mask-seal with hole diameter of 6 mm were attached at the center on both surfaces of the LSO disk. Platinum paste (TR-7907) Tanaka Kikinzoku Kougyo, Ltd., Japan) was attached inside of the hole and then, dried the paste at 373 K for 30 min. Then, 5 ml of the LCO ink was pipetted and pulled into the seal hole. After drying the LCO ink, mask seals on both side of the LSO pellet were removed. Then, both electrodes were attached by heating at 1273 K for 5 h in air.

Before the electrochemical measurements, platinum wire was wound at the side of the pellet and then, small amount of the platinum paste was painted between the LSO pellet and the platinum wire in order to make electrical contact among them.

2.5. Electrochemical Measurements

Electrochemical measurement was performed by three terminal method in one room condition. One platinum wire attached to the side of the LSO pellet was wired to a platinum lead wire. The cell was sandwiched by two platinum meshes fixed on porous alumina plates. Two platinum wires were welded to each mesh to connect a load circuit and sensing circuit of the potentio/galvanostat (R-600, Gamry, USA). Three electrochemical measurement techniques, cyclic voltammetry, electrochemical impedance with- and without d.c. voltage convolution were used for the analysis. The electrochemical measurements were made at the temperature range between 723 K and 1173 under the oxygen partial pressure from 10^{-2} atm to 1 atm. The oxygen partial pressure around the cell was changed using Ar + O_2 gas mixture. The oxygen partial pressure was monitored by zirconia oxygen sensor fixed at the downstream side from the electrochemical cell.

Cyclic voltammetry was measured in air at voltage scan rate of 5 mV/s. Potential difference rage among the working electrode (LCO) and reference electrode (Pt) was between -1.0 V and 1.0 V. Electrochemical impedance was measured in frequency range between 1 MHz and 0.01 Hz depending on the temperature. The electrochemical properties were analyzed based on the extended interfacial conductivity theory [18, 19].

3. Results and discussion

3.1. Chemical reactivity

By comparison of the XRD patterns of the initial mixed powder and the heated powder at 1273 K for 60 h, the LCO and LSO seemed to be equilibrated as two phase coexisting state because the patterns were found to be almost the same and new phase formation was not observed except for a sharpening of the LCO peaks around $2\theta = 33$ to 35 as shown in Fig. 1. Peak width of the XRD is known to be related to the crystallinity and grain size. Therefore, the main reason for variation of the XRD peaks by heating at 1273 K for 60 h is improvement of the crystallinity and grain growth of the LCO powder.

On the other hand, XRD pattern of initial mixed powder by LCO and YSZ changed into different one by heating at 1273 K for 60 h by showing in Fig. 2(a) and (b). New phase showing strong intensity peaks were indexed by the peaks of $La_2Zr_2O_7$ [24] as shown in Fig. 2(a). In addition to the peaks by YSZ and $La_2Zr_2O_7$, weak peaks by Co_3O_4 and LCO were confirmed (Fig. 2(b)). It can be concluded that the LCO is very reactive to YSZ and easily decomposed at 1273 K. Hence, it is difficult to use the LCO as cathode of YSZ electrolyte.

In contract to the case of the LCO/YSZ interface, the LCO is stable even though the LCO is attached to the LSO electrolyte at 1273 K and therefore the LCO is found to be unique candidate as cathode material of LSO electrolyte.

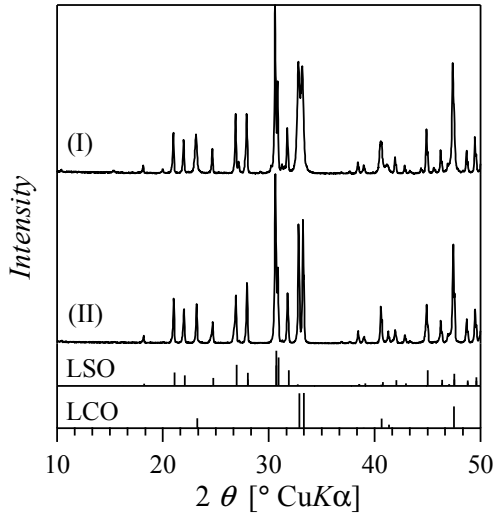

Fig. 1. XRD peaks of LCO and LSO powder mixture. (I) is the peaks of as mixed powder of LCO and LSO and (II) is the sample after heated at 1273 K for 60 h in air. The reported XRD peaks of LCO [23] and LSO [18] are shown for comparison.

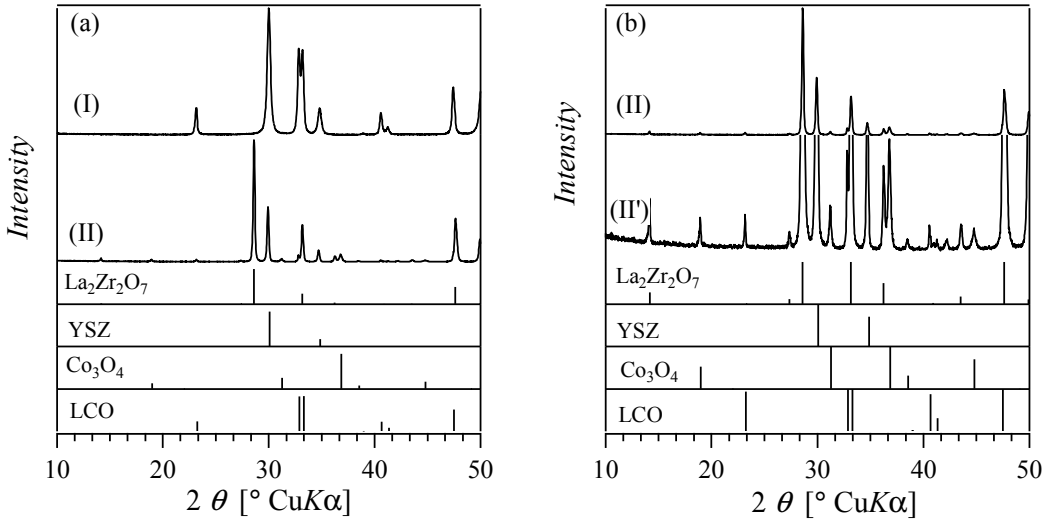

Fig. 2. XRD peaks of LCO and YSZ powder mixture. Whole patterns are shown in (a). Expanded pattern is shown in (b) in order to clealy showing the small peaks. The peaks (I) is the sample as mixture powder and (II) is the peaks of the sample after heating at 1273 K for 60 h in air. The reported XRD peaks of $La_2Zr_2O_7$ [24], YSZ [25] , Co_3O_4 [26], and LCO [23] are ploted for comparison. In figure (b), the expanded pattern of (II) is shown by (II‘). the reported XRD patterns are also expanded in intensity axis.

3.2. Electrochemical impedance under open cell circuit condition

Typical impedance spectra corrected at 1023 K were shown in Fig. 3 as function of oxygen partial pressure. All of the spectra were found to be constructed by two decompressed arcs at high frequency and low frequency region. With respect to the high frequency region arc, it seemed to be distorted signal by the instrument because similar distorted spectrum was measured when the circuit was connected to a test cell constructed by resistors and condenser. Therefore, only the spectra shown in low frequency region were analyzed by the equivalent circuit. The equivalent circuit used in this study is shown in Fig. 4 to fit the obtained spectra. The R_b is the bulk resistance of the electrolyte, R_2 and R_3 are the resistance of the electrode response, respectively. The CPE_2 and CPE_3 are the constant phase element of the electrode response, which are the empirical element to give the Cole-Cole type relaxation [27]. Reason for the separation with two elemental parts by R_2 and CPE_2, and R_3 and CPE_3 is to fit the distorted spectra. It is necessary to emphasize that no clear physicochemical meaning of R_2, R_3, CPE_2, and CPE_3, and is reasonable to consider that sum of these elemental parts should be treated

as electrode impedance ($Z_{electrode}$) as shown in Fig. 4. Therefore, sum of the R_2 and R_3 are treated as electrode resistance (R_E), hereafter.

Based on the interfacial conductivity proposed by Mizusaki *et al*. [28, 29], the interfacial conductivity (σ_E) is defined by

$$\sigma_E = 1/(A \cdot R_E), \quad (1)$$

where A is the electrode area. The relationships between the σ_E and oxygen partial pressure show that the σ_E is almost independent of oxygen partial pressure (Fig. 5). It is necessary to emphasize that the σ_E is not an electrical conductivity but a chemical one [16, 17, 28, 29]. Although it is difficult to conclude the rate determining step by the $p(O_2)$ dependences of σ_E because the measured $p(O_2)$ range is narrow, the $p(O_2)$ dependences on the σ_E becomes weak if about a half of the adsorption site on the metallic electrode surface is fulfilled by the adsorbed oxygen [28, 29]. On the other hand, if the σ_E corresponds to the oxygen permeation by mixed conductive properties in $LaCoO_3$, the σ_E should be proportional to 1/4 power of $p(O_2)$ by considering into the $p(O_2)$ dependence of the partial conductivity of oxide ions in $LaCoO_3$ [30].

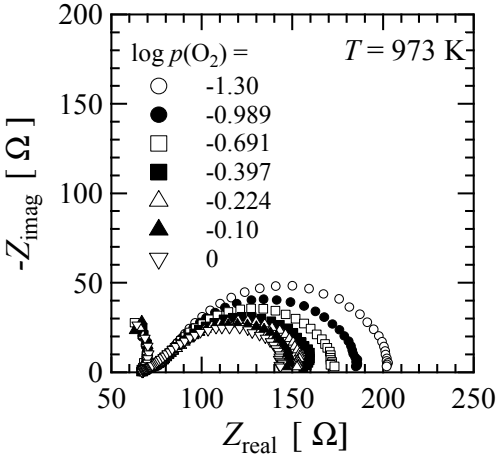

Fig. 3. Impedance spectra of LCO/LSO interface at 973 K as function of oxygen partial pressure. The spectra were corrected under open cell circuit condition.

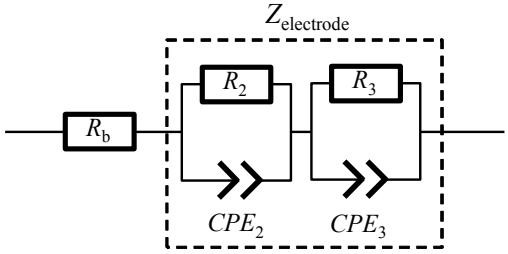

Fig. 4. Equivalent electrical circuit used for evaluation of the electrode resistance. R_b is the resistance of the bulk electrolyte. R_2 and R_3 are the electrode resistance. CPE_2 and CPE_3 are the constant phase element. The electrode impedance ($Z_{electrode}$) is given by broken lined square. Total electrode resistance is given by R_2 and R_3.

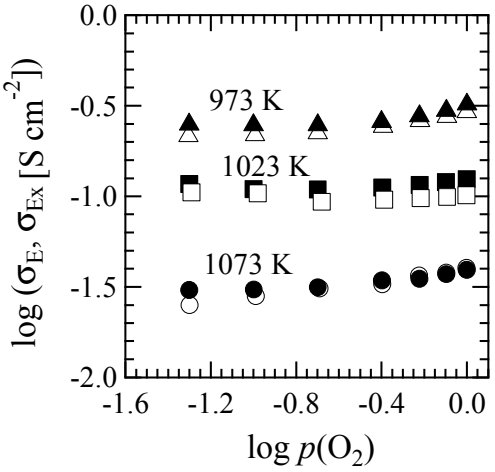

Fig. 5. Interfacial conductivity (σ_E, open marks) and extended interfacial conductivity (σ_{Ex}, closed marks) as function of oxygen partial pressure. The oxygen partial pressure of the σ_{Ex} is evaluated by eqs. (2) and (3).

3.3. Cyclic voltamometry

Relationship between current and potential difference between the working electrode and reference electrode measured by cyclic voltammetry are shown in Fig. 6. In case of solid-state electrochemical system constructed by oxygen ion conductor and electrode, terminal voltage difference between the working electrode and reference electrode ($E_{w\text{-}r}$) is theoretically given when the following two situations are established; (I) steady-state is achieved, and (II) local equilibrium is established [16, 28],

$$E_{w\text{-}r} - E_{op} = i(O^{2-})\, R_b + \eta, \tag{2}$$

where E_{op}, $i(O^{2-})$, and η are the terminal voltage at open cell circuit condition, oxygen ionic current, and overpotential, respectively. Furthermore, the η is presented by,

$$\eta = RT/2F^2 \ln \{a_o(w) / p(O_2, w)^{1/2}\} = RT/4F^2 \ln \{p(O_2) / p(O_2, w)\}.$$

R, T, and F are the gas constant, absolute temperature, and Faraday constant, respectively. The $a_o(w)$ is the oxygen activity under the oxygen ionic current flow at the triple phase boundary among the working electrode, solid electrolyte, and gas phase. The $p(O_2)$ is the oxygen partial pressure at the triple phase boundary under ionic current flow condition. The $p(O_2, w)$ is the oxygen partial pressure at the working electrode side with no current flow condition. In case of this study, $p(O_2, w)$ is equal to 0.21. From the impedance analysis described above, the R_b value was already evaluated, and therefore, we could convert the relationship between the $E_{w\text{-}r}$ and $i(O^{2-})$ as shown in Fig. 6 into the relationship between the η and $i(O^{2-})$ (Fig. 7). Results on the case at LCO/YSZ cell were also plotted for comparison. For the case of LCO/LSO cell, almost no hysteresis was observed by the scan rate at 5 mV/s. On the other hand, clear hysteresis was found in the case of LCO/YSZ cell.

Cathode properties at the LCO/LSO interface is found to be better than the properties at the LCO/YSZ interface by comparison of the η-$i(O^{2-})$ relationships at the same η and temperature condition. One reason is that no insulator phase is formed at the LCO/LSO interface as discussed in section 3.1.

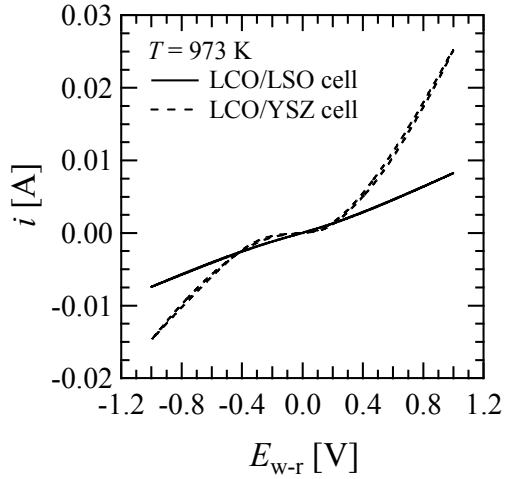

Fig. 6. Variation of the current with terminal voltage between the working electrode (LCO) and reference electrode (Pt) at LCO/LSO cell measured by the cyclic voltammetry.

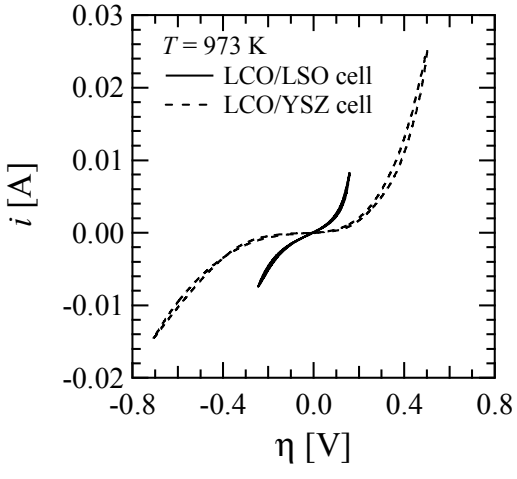

Fig. 7. Variation of the current with overpotential (η) converted by the eq. (2) at LCO/LSO cell.

3.4. Electrochemical impedance with applying d.c. bias

In order to discuss the triple phase boundary situation under steady-state oxygen ionic current flow, impedance spectra were corrected under fixed d.c. bias applied condition. Typical impedance spectra are shown in Fig. 8. The shapes of the spectra are similar to the spectra measured under open cell circuit condition in Fig. 3. Hence, the spectra were analyzed by the same equivalent circuit shown in Fig. 4. The R_E value measured under d.c. bias applied condition is indexed as R_{Ex}. Similarly, the interfacial conductivity under d.c. bias applied condition is named as extended interfacial conductivity (σ_{Ex}) which is presented by [16];

$$\sigma_{Ex} = 1/(A \cdot R_{Ex}). \quad (4)$$

Taking into consideration of the electrochemical impedance model based on the interfacial conductivity theory, the σ_{Ex} is a function of $p(O_2)$ at steady-state current flow condition [16]. If the electrode resistance is determined by the neutral oxygen diffusion on the LCO surface obeying the law of classical irreversible thermodynamics, σ_{Ex} and σ_E values measured by different experiments become the same with each other at the same a_o(w) and temperature. From the plots of σ_{Ex} and σ_E versus $p(O_2)$ (Fig. 5), σ_{Ex} and σ_E show almost the same values. These results indicate that the electrode resistance is not the electric resistance but a kind of chemical resistance by neutral oxygen diffusion by the chemical potential gradient yielding to the classical irreversible thermodynamic process [16]. In order to check an adequacy of this result, we confirmed the total conductivity (σ_t) of the LCO bulk as functions of oxygen partial pressure and temperature (Fig. 9). The $p(O_2)$ dependence on the σ_t shows similar tendency to the previous report [30, 31]. Although the oxygen partial pressure dependence of the σ_t of LCO is similar to the $p(O_2)$ dependence of the σ_E and σ_{Ex}, the temperature dependence of the σ_t is opposite to the dependences of the σ_E and σ_{Ex}. These facts are also supported that the σ_E and σ_{Ex} are not governed by the electric properties in the LCO bulk.

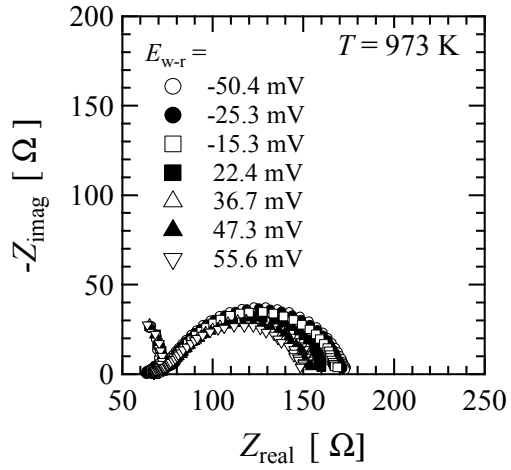

Fig. 8. Impedance spectra corrected under d.c. bias applied conditions using the LCO/LCO cell. The $E_{w\text{-}r}$ indicate that the d.c. bias between the working electrode (LCO) and reference electrode (Pt).

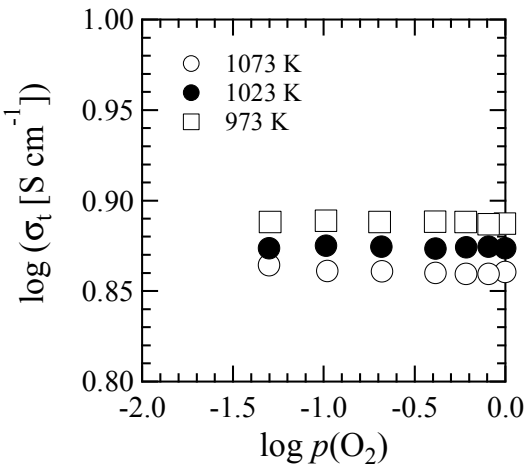

Fig. 9. Relationship between total conductivity (σ_t) of the LCO bulk ceramic and oxygen partial pressure.

4. Summary

Lanthanum cobaltite ($LaCoO_3$) is found to show low chemical reactivity to the lanthanum silicate oxyapatite solid-electrolyte at 1273 K. From solid-state electrochemical measurements, high cathode performance was confirmed at the $LaCoO_3$/lanthanum silicate oxyapatite interface by comparison to the interface at $LaCoO_3$/YSZ. Based on the analysis on the interfacial conductivity theory, the interfacial conductivity evaluated by the impedance spectra measured under open cell circuit condition are found to be the same with the extended interfacial conductivity measured by the d.c. bias applying condition. This result indicates that electrochemical kinetics at the LCO/LSO interface is governed by the LCO surface properties, namely surface diffusion of neutral oxygen and as a result, the relationship between the current and overpotential can be explained based on the interfacial conductivity theory.

References

[1] O. Yamamoto, Y. Takeda, R. Kanno, M. Noda, Perovskite-type oxides as oxygen electrodes for high temperature oxide fuel cells, Solid State Ionics 22 (1986) 241-246.

[2] Y. Takeda, R. Kanno, M. Noda, Y. Tomida, O. Yamamoto, Cathodic polarization phenomena of perovskite oxide electrodes with stabilized zirconia, J. Elecctrochem. Soc. 134 (1987) 2656-2661.

[3] Y. Teraoka, T. Nobunaga, K. Okamoto, N. Miura, N. Yamazoe, Influence of constituent metal cations in substituted $LaCoO_3$ on mixed conductivity and oxygen permeability, Solid State Ionics 48 (1991) 207-212.

[4] C.H. Chen, H. Kruidhof, H.J.M. Bouwmeester, A. J. Burgraaf, Ionic conductivity of perovskite $LaCoO_3$ measured by oxygen permeation technique, J. Appl. Electrochem. 27 (1997) 71-75.

[5] B.C.H. Steel, Materials for IT-SOFC stacks. 35 years R&D: the inevitability of gradualness?, Solid State Ionics. 134 (2000) 3-20.

[6] O. Yamamoto, Solid Oxide Fuel Cells: fundamental aspect and prospects. Electrochim. Acta. 45 (2000) 2423-2435.

[7] H.J.M. Bouwmeester, Dense ceramic membrane for methane conversion, Catal. Today. 82 (2003) 141-150.

[8] H. Yokokawa, N. Sakai, T. Kawada, M. Dokiya, Thermodynamic analysis of reaction profile between $LaMnO_3$ (M = Ni, Co, Mn) and ZrO_2, J. Electrochem. Soc. 138 (1991) 2719-2727.

[9] J.A. Labrincha, J.R. Frade, F.B.B. Marques, $La_2Zr_2O_7$ formed at ceramic electrode/YSZ contacts, J. Mater. Sci. 28 (1993) 3809-3815.

[10] F.M. Figueiredo, J.A. Labrincha, J.R. Frade, F.M.B. Marques, Reactions between a zirconia-based electrolyte and $LaCoO_3$-based electrode materials, Solid State Ionics 101-103 (1997) 343-349.

[11] S. Nakayama, H. Aono, Y. Sadaoka, Ionic conductivity of $Ln_{10}(SiO_4)_6O_3$ (Ln=La, Nd, Sm, Gd, and Dy), Chem. Lett. 24 (1995) 431-432.

[12] S. Nakayama, T. Kageyama, H. Aono, Y. Sadaoka, Ionic conductivity of lanthanoid silicates, $Ln_{10}(SiO_4)_6O_3$, (Ln=La, Nd, Sm, Gd, Dy, Y, Ho, Er and Yb), J. Mater. Chem. 5 (1995) 1801-1805.

[13] S. Nakayama, M. Sakamoto, Electrical properties of new type high oxide ionic conductor $RE_{10}Si_6O_{27}$ (RE = La, Pr, Nd, Sm, Gd, Dy), J. Eur. Ceram. Soc. 18 (1998) 1413-1418.

[14] H. Yoshioka, High oxide ion conductivity in Mg-doped $La_{10}Si_6O_{27}$ with apatite-type structure. Chem. Lett. 33 (2004) 392-393.

[15] A. Orera, P.R. Slater, New chemical synthesis for solid oxide fuel cells, Chem. Mater. 22 (2010) 675-690.

[16] K. Kobayashi, Y. Sakka, Theoretical modeling of electrode impedance for an oxygen ion conductor and metallic electrode system based on the interfacial conductivity theory, Solid State Ionics 232 (2013) 49-57.

[17] K. Kobayashi, K. Terabe, T. Sukigara, Y. Sakka, Theoretical modeling of electrode impedance for an oxygen ion conductor and metallic electrode system based on the interfacial conductivity theory. Part II: Case of the limiting process by non-steady-state surface diffusion, Solid State Ionics 249-250 (2013) 78-85.

[18] K. Kobayashi, Y. Matsushita, N. Igawa, F. Izumi, C. Nishimura, S. Miyoshi, Y. Oyama, S. Yamaguchi, Water-based sol-gel synthesis and crystal structure refinement of lanthanum silicate apatite. Solid State Ionics 179 (2008) 2209-2215.

[19] K. Kobayashi, T.S. Suzuki, T. Uchiskoshi, Y. Sakka, Low-temperature formation of Ln silicate oxyapatite (Ln = La and Nd) by the water-based sol-gel method, Solid State Ionics 204-205 (2011) 91-96.

[20] K. Kobayashi, Y. Sakka, Phase relationships in the quasi-ternary $LaO_{1.5}$-SiO_2-MgO system at 1773 K, Sci. Tech. Adv. Mater. 13 (2012) 045006 (12pp).

[21] J. Kinnunen, B. Wennerstrand, Some further applications of xylenol orange as an indicator in the EDTA titration, Chemist-Analyst. 46 (1957) 92-93.

[22] K. Kobayashi, C. Nishimura, Electrical transport and electric power generation properties of lanthanum-silicate oxyapatite ceramics prepared by asol-gel method, ECS Trans. 25 (2009) 1785-1790.

[23] O. Haas, R.P.W. J. Struis, J.M. McBreen, Syncrotron X-ray absorption of $LaCoO_3$ perovskite, J. Solid State Chem. 177 (2004) 1000-1010.

[24] E.J. Harvey, K.R. Whittle, G.R. Lumpkin, R.I. Smith, S.A.T. Redfern, Solid Solubility of (La, Nd)$_2$(Zr, Ti)$_2O_7$ phases deduced by neutron diffraction, J. Solid State Chem. 178 (2005) 800-810.

[25] M. Walter, C. Nästren, J. Somers, R. Jardin, M.A. Denecke, B. Brendebach, Local atomic structure of a zirconia-based americium transmutation fuel, J. Solid State Chem. 180 (2007) 3130-3135. YSZ crystal structure

[26] M. Casas-Cabanas, G. Binotto, D. Larcher, A. Lecup, V. Giordani, J.-M. Tarascon, Defect chemistry and catalytic activity of nanosized Co_3O_4, Chem. Mater. 21 (2009) 1939-1947.

[27] J.R. Macdonald, Note on the parameterization of the constant-phse admittance element, Solid State Ionics 13 (1984) 147-149.

[28] J. Mizusaki, K. Amano, S. Yamauchi, K. Fueki, Electrode reaction at Pt, O_2(g)/stabilized zirconia interfaces. Part I: Theoretical consideration of reaction model, Solid State Ionics 22 (1987) 313-322.

[29] J. Mizusaki, K. Amano, S. Yamauchi, K. Fueki, Electrode reaction at Pt, O_2(g)/stabilized zirconia interfaces. Part II: Electrochemical measurements and analysis, Solid State Ionics 22 (1987) 323-330.

[30] A.N. Petrov, A.Y. Zuev, A.I. Vylkov, D.S. Tsvetkov, Equilibrium of point defects and charge transfer in lanthanum cobaltite, Russ. J. Phys. Chem. 80 (2006) S128-S133.

[31] A.N. Petrov, V.A. Cherepanov, A.Y. Zuev, Thermodynamics, defect structure, and charge transfer in doped lanthanum cobaltites: an overview. J. Solid State Electrochem. 10 (2006) 517-537.